

Surface Micro Defect Detection of Tapered Rollers Based on Laser Diffraction

Li Cao¹, Shuncong Zhong^{1,2*}, Qiukun Zhang¹ and Xinbin Fu³

¹Laboratory of Optics, Terahertz and Non-destructive Testing & Evaluation, School of Mechanical Engineering and Automation, Fuzhou University, Fuzhou 350108, China

²Fujian Key Laboratory of Medical Instrument and Pharmaceutical Technology, Fuzhou 350108, P.R. China

³Xiamen Special Equipment Inspection Institute, Xiamen 361000, P. R. China

Abstract

A method based on laser diffraction was reported to improve the defect recognition accuracy of surface micro defect detection of tapered rollers. According to Fraunhofer diffraction theory, the fluctuations of the width of a tiny slit can be transformed to obvious changes of diffraction fringes, which can be employed to measure the micro surface defect of tapered rollers. These optical diffraction fringes were captured by a CCD camera, and subsequently were transmitted to a developed image processing system. The system includes image de-noising based on anisotropic diffusion, automatic extraction of fringe center lines by the derivative-sign binary image method, and analysis of the extracted fringe center lines for automatic defect detection. The experimental results demonstrated that the proposed method could magnify defect effect and therefore improve the accuracy of defect detection, making it attractive for industrial applications on tapered roller defect detection.

Keywords: Laser diffraction; Surface micro defect detection; Tapered roller; Image processing

Introduction

Recently, due to high precision, high quality, and high speed demand of mechanical equipment becomes higher and higher, the bearing plays an increasingly prominent role in industries. Rolling element (known as roller), the most important one of the rolling bearing components, is crucial to the rotating accuracy, kinematic performance, and working life of the bearing. For a tapered roller bearing, the roller is even more important since it acts as bearing and transmitting role, which makes great influence on working performance [1]. According to the experiments, surface roughness of the bearing roller takes fifty percent influence of the every factor: the lifetime, working noise, and rotating accuracy [2]. Thus, it can be seen that any surface micro defect of the bearing may seriously affect the working performance. Therefore, strict quality testing to the surface of the roller is necessary. Improving this detection precision is a problem demanding prompt solution for bearing industries.

At present, most bearing manufacturers adopt artificial visual inspection method. However, it is inefficiency and works on low precision. This method is also unable to overcome the error due to human fatigue. It no longer meets the requirement of modern industry. Magnetic particle flaw detection [3] is a common way for nondestructive testing. It can detect small defects on the surface as well as near the surface of the work piece, but it is not suitable to detect shallow and wide faults. Eddy current testing technique [4] is good for surface crack detection, but it is not sensitive to other cosmetic defects, and the anti-jamming performance of the system is poor. Thus, missing detection and false detection are unavoidable if eddy current technique is used. Acoustic vibration [5,6] is mainly used to test the bearing roller surface crack; however, it is only suitable for some defect detection. Detection based on CCD system for testing the roller surface defect has high precision, fast processing speed, high resolution, and strong anti-interference ability, etc. That makes it become the major trend of the current research work. However, the method lacks comprehensive knowledge of defect generation mechanism and presentation; also, there is no general digital signal processing

platform and pattern recognition algorithm suitable for the detection [7]. With the development of computer technology, neural theory and pattern recognition technology has been being mature. Machine vision detection technology will make due contributions to the detection of the surface defects of bearing rollers. Therefore, the on-line automatic detection system based on machine vision technology to detect bearing roller surface defect is particularly important in the field. However, the ability of machine vision detection technology to test surface tiny defect of high precision bearing roller is limited. In the present work, laser diffraction measurement technique [8] was employed for surface micro defect detection of tapered rollers and it improved the accuracy of defect detection by magnifying defect effects.

Defect Detection Methodology for Tapered Rollers

Theory of laser diffraction measurement technique

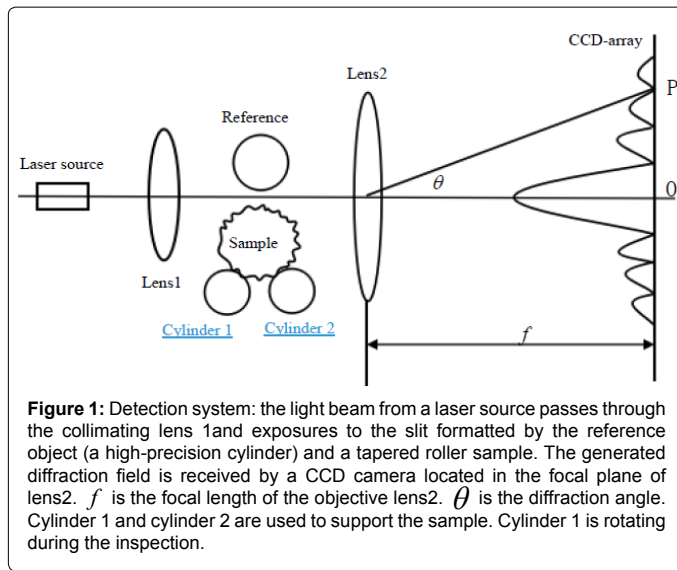
Laser diffraction technique, based on Fraunhofer diffraction [9], is non-contact detection method with good stability and high precision. The measurement system employed in the present work is shown in Figure 1. The light beam from a laser source passes through the collimating lens and exposures to the slit formatted by the reference object (a high-precision cylinder) and a tapered roller sample. The generated diffraction field is received by a CCD camera located in the focal plane of lens2. The computer collects and records the information of the diffraction stripes; subsequently the image is processed by a developed image processing system. The surface defects of the tapered

***Corresponding author:** Shuncong Zhong, Laboratory of Optics, Terahertz and Non-destructive Testing & Evaluation, School of Mechanical Engineering and Automation, Fuzhou University, Fuzhou 350108, China, Tel: +86 591 87893; E-mail: Chinazhongshuncong@hotmail.com

Received September 28, 2015; **Accepted** November 16, 2015; **Published** November 20, 2015

Citation: Cao L, Zhong S, Zhang Q, Fu X (2015) Surface Micro Defect Detection of Tapered Rollers Based on Laser Diffraction. *Sensor Netw Data Commun* 4: 129. doi:10.4172/2090-4886.1000129

Copyright: © 2015 Cao L, et al. This is an open-access article distributed under the terms of the Creative Commons Attribution License, which permits unrestricted use, distribution, and reproduction in any medium, provided the original author and source are credited.



roller can be identified by analyzing the spacing between the k -th dark stripe and 0-th stripe.

The experimental setup for laser diffraction measurement system is shown in Figure 2. The sample is supported by cylinder 1 and cylinder 2. Cylinder 1 controlled by the driving motor is rotating when the detection system works. The sample will rotate during the inspection by the frictional force between cylinder1 and the sample. Noted that the rotation is driven by the motor by gear transmission. However, the limitation of this system is that the ends of the tapered roller sample cannot be tested because they are used to contact the reference to generate the slit.

The light intensity received by a CCD camera and the coordinate position of k -th diffraction dark stripe can be calculated approximately by the following formulas:

$$I = I_0 (\sin^2 \beta) / \beta^2 \quad (1)$$

$$X_k = \frac{kf\lambda}{d} \quad (2)$$

Where λ is the wavelength of the laser source; f is the focal length of lens2; $\beta = (\pi d / \lambda) \sin \theta$, and I_0 is the light intensity when the diffraction angle $\theta=0$. The width of the slit d can be calculated as

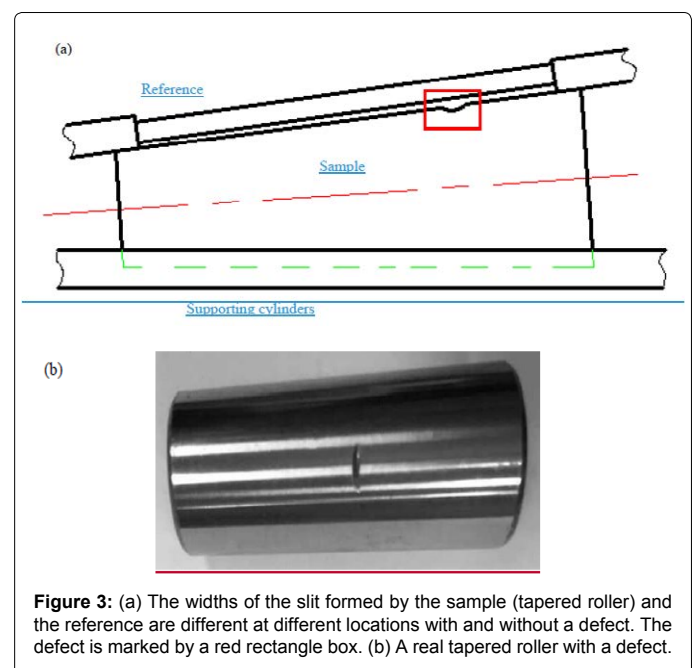
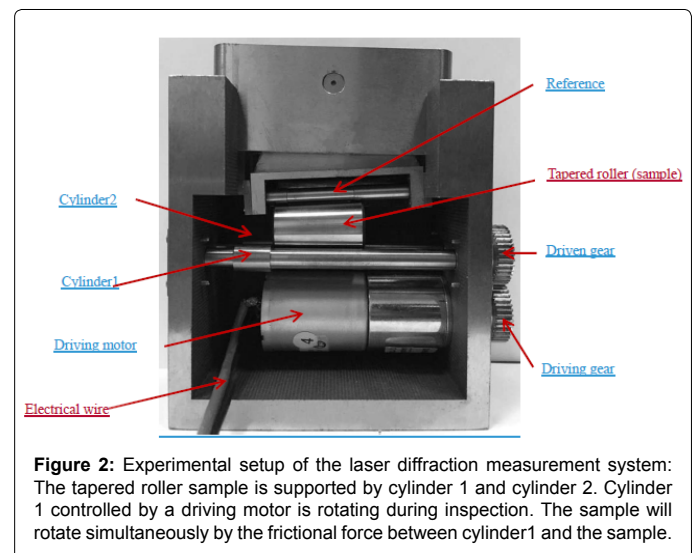
$$d = \frac{kf\lambda}{X_k} \quad (3)$$

If there exists a defect on the surface of a tapered roller (sample), as shown in Figure 3a, the diffraction fringes will be different in different locations when the slit is formatted by the contour lines of the sample and the reference. Due to the slit widths are different at defect and no defect locations, the coordinates of the k -th stripe will have enlarged gap in the corresponding locations. Figure 3b shows a real tapered roller with a defect (dented surface), which is used in the experiment. Detection of other defects will be considered as our future work. Figure 4a and 4b show the diffraction fringes captured from the locations where a defect and no defect exists. There is large fluctuation in the fringe marked by a red rectangle box, which results from the defect located on the surface of the tapered roller.

From Equation (2), the amplification factor of diffraction A_f can be deduced as

$$A_f = \frac{\delta X_k}{\delta d} = \frac{kf\lambda}{d^2} \quad (4)$$

In our experiment, 3-th dark stripe was used, i.e., $k=3$. A lens with focus length of $f=25$ mm and a light with wavelength of $\lambda=0.63 \mu\text{m}$ were employed. For the width of the slit, the suggested value of d is between 0.01 and 0.5 mm [10]. Since a smaller slit width will result in more clear diffraction and higher amplification factor, we set the width of the slit to 0.02 mm. So, the amplification factor of diffraction A_f is about 118, i.e., the slit width could be amplified by 118.2 times. For the measurement system, the resolution in fact depends on the pixel size of CCD and also the precision of the image processing algorithm used. The CCD camera we used is DC140M (ShenZhen D-image Technology Co.,Ltd., China) whose pixel size is $4.65 \times 4.65 \mu\text{m}$. In our current setup, we could obtain the defect information from at least 4 pixels of the CCD. Therefore, the resolution of X_k is $18.6 \mu\text{m}$ and subsequently the



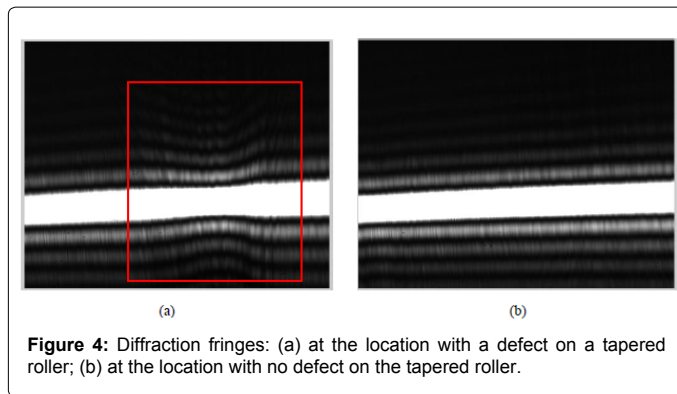


Figure 4: Diffraction fringes: (a) at the location with a defect on a tapered roller; (b) at the location with no defect on the tapered roller.

minimum recognizable defect depth of our system is about $0.176 \mu\text{m}$ which can be calculated using Equation (4).

Derivative-sign binary image method

From Figures 4a and 4b, the defect can be identified automatically by extracting fringe center lines and analyzing its characteristic. At the present work, derivative-sign binary image (DSBI) [11,12] method was employed to extract the fringe center lines. From Equation (1), we know that the derivatives in the fringe normal direction on both sides of a fringe center line have opposite signs whilst the signs of the normal derivatives in the area between adjacent dark fringes and bright fringes center lines are the same. This feature is always true for both dark and bright fringes, no matter how dark and how bright the fringe and no matter what the fringe density. The feature of diffraction fringes in Figure 4 is the same as the feature of interference fringe patterns described in ref [11]. Hence, this feature is also our criterion for constructing a binary image. In the binary image, we set the points equal to the dark value if the derivative-sign is negative, or to equal the bright value, as shown in Figure 5.

The boundaries of the binary fringes are the center lines of the original fringes without deviation. The points of the derivative-sign binary-fringe image can be presented as

$$G_{ij} = \begin{cases} B & \partial G / \partial r|_{ij} \geq 0 \\ 0 & \partial G / \partial r|_{ij} < 0 \end{cases} \quad (5)$$

where G_{ij} is the gray level at point ij for the binary image; G is the gray level of the original image; r is the position vector in the direction perpendicular to the local fringe tangent, with the positive direction defined in Figure 5; B is the bright value of the binary image. We take the derivative signs as the judgment for that they are more sensitive to the gray-level variation of fringes. The derivatives of equation (5) are derived by a nominal derivative algorithm as

$$\frac{\partial G}{\partial r}|_j = \sum_{r=1}^n (G_{j+r} - G_{j-r}) \quad (6)$$

where G_{ij} is the gray level of a current point and G_{j+r} is the gray level of the r -th point counted from the current point in the local fringe normal direction. The n normally takes a value of 2 or 3, depending on the fringe density.

In order to present the result of DSBI, a simulation was done according to Fraunhofer diffraction of single slit. Figure 6a is the diffraction fringe pattern, and Figure 6b is the corresponding derivative-sign binary-fringe image. The Figures demonstrate that the

boundaries of the binary fringes are just the center lines of the original fringes without any deviation.

Extraction of binary-fringe boundaries

A new method is proposed in the present work for extracting binary-fringe boundaries. Because the fringes of images are not closed and are along the horizontal direction, the edge pixel points of the derivative-sign binary-fringe image have the following property

$$G_j = B \ \& \ |G_{i+1j} - G_{i-1j}| = B \quad (7)$$

This feature can be the criterion for extracting binary-fringe boundaries. We set the points, in the binary images obtained by DSBI, meeting the property expressed by equation (7) to equal bright value, or to equal the dark value. There is a problem that the noise pixel points from the binary image may meet the requirement. However, the problem can be avoided by filtering the binary image before extracting binary-fringe boundaries. In this work, we adopted morphological filtering method [13].

Image de-noising based on anisotropic diffusion

Many filtering methods treated the high frequency component as noise, which sometimes will result in losing the edge information of image. Researchers hoped to find methods that could distinguish the high frequency characteristics of image from noise, and then nonlinear diffusion methods arose. Perona and Malik first proposed nonlinear

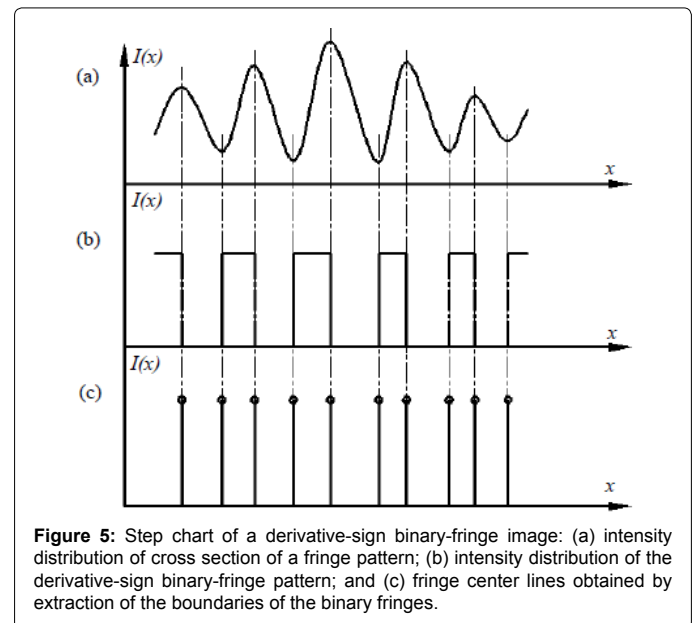


Figure 5: Step chart of a derivative-sign binary-fringe image: (a) intensity distribution of cross section of a fringe pattern; (b) intensity distribution of the derivative-sign binary-fringe pattern; and (c) fringe center lines obtained by extraction of the boundaries of the binary fringes.

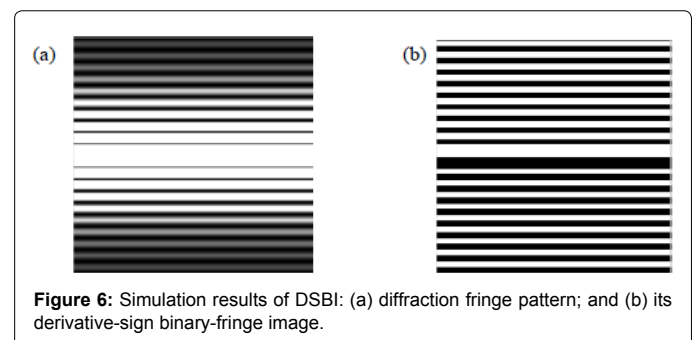


Figure 6: Simulation results of DSBI: (a) diffraction fringe pattern; and (b) its derivative-sign binary-fringe image.

diffusion equation: P-M equation [14]. It is mathematically formulated as a diffusion process, and it encourages intra-region smoothing in preference to smoothing across the boundaries. The estimation about local image structure is guided by knowledge about the statistics of the noise degradation and the edge strengths.

The following is the theory of the anisotropic diffusion proposed by Perona and Malik.

We assumed that I_0 represents a piece of gray image, $I_0(x,y)$ is the gray level at point (x,y) of the image. Introducing the time factor t , the anisotropic diffusion equation used to modify the noisy image can be expressed as

$$\begin{cases} \frac{\partial I}{\partial t} = \text{div}(c(|\nabla I|) \cdot \nabla I) \\ I(x, y, 0) = I_0(x, y) \end{cases} \quad (8)$$

The function $c(|\nabla I|)$ is a monotonically decreasing function called diffusion coefficient and is anisotropic [14]. To achieve the above properties, $c(|\nabla I|)$ needs to satisfy the following conditions:

$$\begin{cases} c \longrightarrow 0 & \text{for } |\nabla I| \longrightarrow \infty \\ c \longrightarrow 0 & \text{for } |\nabla I| \longrightarrow 0 \end{cases}$$

Perona and Malik proposed two functions for $c(|\nabla I|)$ expressed by

$$c(|\nabla I|) = \exp\left(-\left(\frac{|\nabla I|}{k}\right)^2\right) \quad (9)$$

$$c(|\nabla I|) = \frac{1}{1 + \left(\frac{|\nabla I|}{k}\right)^2} \quad (10)$$

where k is the edge magnitude parameter also is called smoothing parameter. Equation (9) is called 'option 1' and equation (10) is called 'option 2' when the anisotropic diffusion is implemented. The diffusion coefficient in equation (9) favors high-contrast edges over low-contrast ones; the diffusion coefficient in equation (10) favors wide regions over smaller ones [14].

Thus, anisotropic diffusion is an efficient nonlinear technique for simultaneously performing contrast enhancement and noise reduction. It preserves the edges by allowing no diffusion over the edges but allowing diffusion parallel to the edges. This is an iterative equation on the initial condition of image I_0 . The solution $I(x,y,t)$ is the new image obtained after t times iteration, and stop the iterating process when getting the satisfied image.

Results and Discussions

The image processing of diffraction fringes is implemented through the following five steps: 1) Image de-noising based on anisotropic diffusion; 2) Making the DSBI and filtering the DSBI by morphology filtering method; 3) Extracting binary-fringe boundaries; 4) Extracting the 0-th and k -th fringe center lines; 5) Analyzing the result obtained from step 4).

Figures 7a and 7b show two captured diffraction fringes. Figure 7a is different from Figure 7b since it has a fluctuation, which reflects there is defect on the surface of the tapered roller. Five-step signal processing method is employed to process the images.

The de-noising results based on anisotropic diffusion is shown in

Figure 8. The derivative-sign binary images of Figure 8a and 8b after filtering by morphology method are shown in Figure 9. In order to illustrate the advantage of this de-noising method based on anisotropic diffusion, the result of block-matching 3D filtering (BM3D) [15], one of the state-of-the-art de-noising methods, is shown in Figure 10. The result shown in Figure 10 is poor than the one shown in Figure 9. The

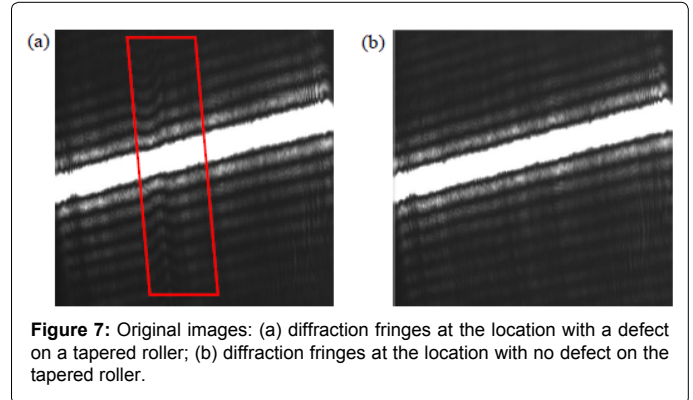


Figure 7: Original images: (a) diffraction fringes at the location with a defect on a tapered roller; (b) diffraction fringes at the location with no defect on the tapered roller.

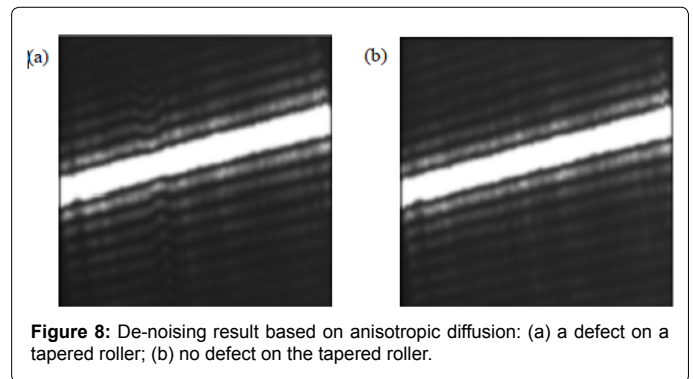


Figure 8: De-noising result based on anisotropic diffusion: (a) a defect on a tapered roller; (b) no defect on the tapered roller.

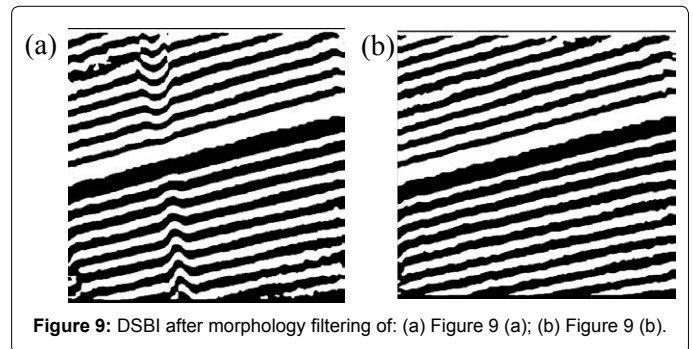


Figure 9: DSBI after morphology filtering of: (a) Figure 7(a); (b) Figure 7(b).

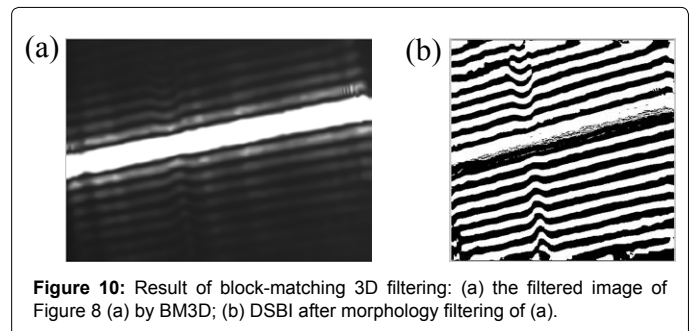


Figure 10: Result of block-matching 3D filtering: (a) the filtered image of Figure 8(a) by BM3D; (b) DSBI after morphology filtering of (a).

DSBI of the original images are shown in Figure 11. It can be seen that there is much noise in Figures 9 (a), 10 (b), and 11 (a), we can make a conclusion that the de-noising method based on anisotropic diffusion is more consistent with our filtering purpose than the BM3D since it not only preserves the useful information but also have better filtering performance.

After making the DSBI and filtering the DSBI by morphology method, the binary-fringe boundaries are extracted by the method proposed in section 2.3, as shown in Figure 12. In order to analyze the fluctuation characteristic of the fringes, the center lines of 0-th stripes and 3-th dark stripes are extracted, as shown in Figure 13.

To recognize the defect automatically, the analyzing process could be described in two steps as following: 1) Extraction of the gray value and the horizontal coordinates of Figure 8 at the location of center lines of 0-th and 3-th dark stripes. In this step, we discarded the beginning and ending data of the center lines for that they were contaminated by the background. 2) Correction of the obtained curves by making them not slanted and by subtracting the dc component. Subsequently, the distance of the two corrected curves is calculated. The result is shown in Figure 14. It can be found that there is a peak in the distance curve as shown in Figure 14 (a). This indicates a defect exists on the tapered roller. If a proper threshold is set, defect detection of tapered roller could be achieved.

Conclusions

In the present work, we have demonstrated a methodology for detect detection of the surface micro defect on tapered roller. Experimental results show that the method can detect the defect accurately. The whole implementation process is automatic and the image processing method is very simple and robust. According to Fraunhofer diffraction

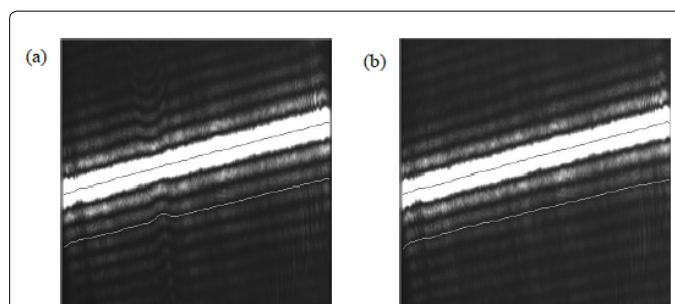


Figure 13: Center lines of 0-th and 3-th dark stripes. The lines are shown on the original images.

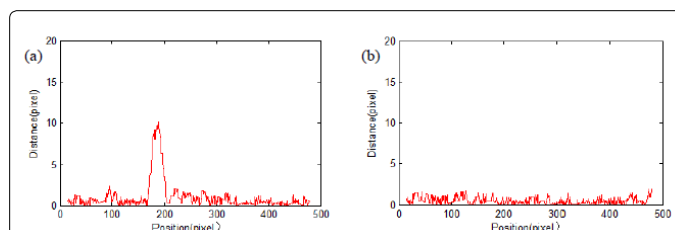


Figure 14: Distance of the corrected curves of center lines extracted from 0-th and 3-th dark stripes using (a) the center lines obtained in Figure 13 (a); and using (b) the center lines obtained in Figure 13(b).

theory, the fluctuations of the width of the tiny slit can be transformed to obvious changes of the coordinates of the fringes, which can be employed to measure the micro surface defect of the rollers. These optical diffraction fringes were captured by CCD-array, and then were transmitted to a developed image processing system, which includes image de-noising based on anisotropic diffusion, automatic extraction of fringe center lines by the derivative-sign binary image method, and analysis of the extracted fringe center lines for automatic defect detection on tapered roller. Our approach has great potential in real application in surface micro defect detection of taper roller and other cylindrical components.

Acknowledgements

We gratefully acknowledge support from the National Natural Science Foundation of China (51005077), the Fujian Provincial Excellent Young Scientist Fund (2014J07007, 2011J06020), the Specialised Research Fund for the Doctoral Program of Higher Education, the Ministry of Education, P. R. China (20133514110008), the Ministry of Health, P.R. China (WKJ-FJ-27) and Fujian Provincial Natural Science Foundation (2015J01234).

References

1. Wenlong W (2013) Automatic detection system for detecting the surface of tapered roller. Changchun University of Science and Technology.
2. Wen H, Yan W, Jianying Lv (2005) Analysis of factors influenced on grinding surface roughness of tapered roller. *J. Bearing* 12: 15-16.
3. Stadthaus M (1991) Investigations on magnetic hand-yokes for the magnetic particle inspection. *J. Materials Testing*: 88-91.
4. Chuanbin P, Huifen G (2002) Research on surface defects detection for railway vehicle bearing roller. *J. Sci-Tech Information Development & Economy* 12: 169-171.
5. Jingliang Z, Zhixi L, Yaozhi H (2006) Nondestructive detection of roller bearing with acoustic vibration. *J. Mechanical & Electrical Technology* 29: 36-37.
6. Jingliang Z, Zhixi L, Yaozhi H (2007) Data acquisition and processing of nondestructive testing for bearing roller. *Journal of Fujian University of Technology* 5: 79-82.
7. Fangqing J (2007) Research on Surface Defects Detection for Steel Strips Based on Machine Vision [D]. 2007: 68-69.

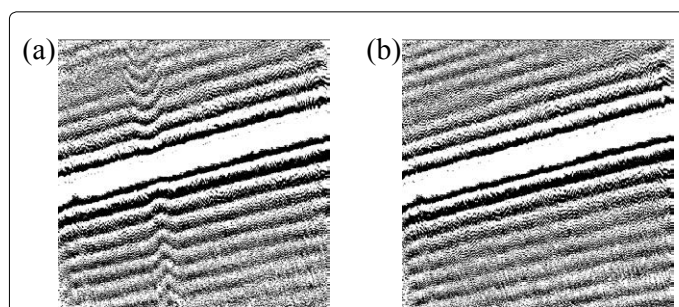


Figure 11: (a) DSBI of the original image shown in Figure.7 (a); (b) DSBI of the original image shown in Figure 7 (b).

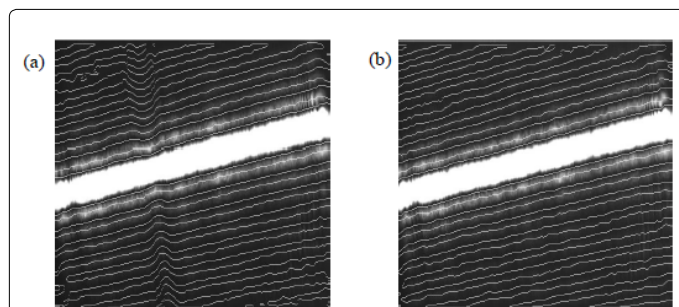


Figure 12: Extracted fringe skeletons of Figure 9. The skeletons are shown on the original images.

8. Suhong D, Hui F, Huisheng W (2005) Study of the Radial Beat Measurement System of High Speed Drilling Machine Using CCD Laser Diffraction. *J Measurement & Control Technology* 24: 71-72.
9. Xiaoi G, Xiangning L, Jiabi C (2002) System of thin cylinder diameter measurement by Fraunhofer diffraction with digital camera. *M. College Physics* 21: 36-39.
10. Changku S, Mingxia H, Peng W (2008) *Laser measurement technology*. M Tianjin: Tianjin University press pp: 84-85.
11. Yu Q, Andresen K (1994) Fringe orientation maps and 2D derivative-sign binary image methods for extraction of fringe skeletons. *J. Appl. Opt* 33: 6873-6878.
12. Yu Q, Liu X, Sun X (1998) Generalized spin filtering and improved derivative-sign binary image method for extraction of fringe skeletons. *J. Appl. Opt.* 37: 4504-4509.
13. Cheng F, Venetsanopoulos AN (2000) Adaptive morphological operators, fast algorithms and their applications. *Pattern Recognit* 33: 917-933.
14. Perona, Malik J (1990) Scale-space and edge detection using anisotropic diffusion. *J. IEEE Trans on PAMI* 12: 629-639.
15. Dabov K, Foi A, Katkovnik V, Egiazarian K (2006) Image de-noising with block-matching and 3D filtering. *J Proc. SPIE Electronic Imaging: Algorithms and Systems* 1: 6064A-30.